

Dynam ical and chem ical effects of FR II radio sources on the intra-cluster m edium

M .H uarte-E spinosa,^{1,2} M .K rause,^{1,2,3} P .A lexander,¹ and C .R .K aiser⁴

¹A strophysics G roup, C avendish Laboratory, 19 J. J. T hom son Ave., C am bridge CB3 0HE, U K

²M ax-P lanck-Institut für E xtraterrestrische P hysik, G iessenbachstrasse, 85748 G arching, G erm any

³U niversitätssternwarte M ünchen, Scheinerstr. 1, 81679 M ünchen, G erm any

⁴School of P hysics and A stronomy, U niversity of Southam pton, Southam pton SO17 1BJ, U K

Received 20 February 2024

A B S T R A C T

We investigate the effects of intermittent strong jets from an Active Galactic Nuclei (AGN) of a massive galaxy in the core of a cool core galaxy cluster, on the dynamics and metal distribution of the intra-cluster medium (ICM). We use a simple model for the metal distribution within the host galaxy which includes metal injection via star formation. We carry out 2D axisymmetric hydrodynamic simulations of these systems. After having established a cooling flow, two light jets are injected in opposite directions with a range of (intermittent) active phases. We follow the time evolution of the system from the jets' active phases up to 3 Gyr. The general metallicity evolution for all our simulations is very similar on large-scales. The convective flows driven by the jets advect gas and metals from the central galaxy to distances beyond 1.5 Mpc within the cluster. Intermittent jets are able to distribute metals to greater radii. The metal injection has effects on the general metal abundances present in the ICM, the faster the metal replenishment time the higher the metal abundance. Although metallicity gradients in the very central regions of cool core clusters are likely to be shaped by less-energetic phenomena, we find evidence in our simulations for metallicity gradients similar to those observed out to ~ 400 kpc radius. The metal distribution details of the central galaxy have no effects on the dynamical evolution of the ICM metals.

Key words: hydrodynamics { galaxies: jets { methods: numerical { X-rays: galaxies: clusters.

1 I N T R O D U C T I O N

The abundance and distribution of heavy elements (metals) in the intra-cluster medium (ICM) holds information about the history of galaxy clusters (clusters from now on). Metals formed as a result of star formation in the cluster galaxies must be transported into the ICM and a variety of mechanisms are possible, for example galactic-scale winds, or outflows driven by Active Galactic Nuclei (AGN). X-ray spectroscopic observations provide a direct probe of metallicity gradients in the ICM. Many clusters show an approximately flat metallicity distribution, of about a third of the solar (Z), out to megaparsec distances from the cluster core (De Grandi & Molendi 2001). Moreover, the metallicity profiles of cool core intermediate redshift ($0.1 \leq z \leq 0.35$) clusters, particularly those that show no evidence of shocks associated with mergers, have an abundance excess of the order $0.45 \pm 0.55 Z$ at their cores (De Grandi & Molendi 2001;

Bakke et al. 2007; Leccardi & Molendi 2008). High resolution Chandra X-ray observations of the core of Hydra A, show that metals in the central regions were formed by different stellar populations (David et al. 2001), with a metal replenishment time of the order of 60 Myr^{-1} over a period of 1 Gyr. Similar results are found for other clusters as well (Molendi 2004).

Over recent years there has been a growing consensus that radio galaxies have a significant impact on the cluster environment (see McNamara & Nulsen 2007 for a recent review). Jets from radio-loud AGN provide an ideal mechanism for coupling the energy output from the AGN to the surrounding gas, both via heating by the bow shock (Binney & Tabor 1995; Kaiser & Alexander 1999; Reynolds, Heinz & Begelman 2001; Alexander 2002; Krause 2003), but also by driving gas from the core during both the active phase of the jet (e.g., Alexander 2002), but also as the buoyant remnant of bubbles of the radio-source cocoons rise through the cluster gas (e.g., Churazov et al. 2001; Banton et al. 2001; Reynolds et al. 2001). The effects can

² E-mail: mh475@marao.cam.ac.uk

be very long lasting as a large-scale convective flow can be established by the rising bubbles (Basson & Alexander 2003). These flows have important effects on the entropy and energy of the central ICM (see e.g., Kaiser et al. 2005 and references therein), and can transport metals from the core to radii of order a megaparsec within the cluster (Renzini 2004; Heath, Krause & Alexander 2007). Moreover, the bubbles are inferred to produce hydrodynamic turbulence in the ICM (Rebusco et al. 2006). These processes may well be linked to the cluster-wide feedback with infall of cooling gas triggering the AGN activity (e.g., Binney & Tabor 1995; Kaiser & Binney 2003; Shabala et al. 2008). The observed lack of evolution of the ICM metallicity out to redshift of order 1 (Carilli et al. 2001; Mushotzky & Loewenstein 1997; Leccardi & Molendi 2008), suggests that metal advection took place at or before a redshift of unity. Furthermore, the metallicity gradients in the ICM also suggest that the metals were expelled from the dominant central cluster galaxy rather than from ram-pressure stripping of cluster galaxies in general (Renzini 2004). Supernovae do not provide sufficient energy for that process and an attractive alternative are powerful radio galaxies (Heath et al. 2007).

In this paper we examine the advection of metals driven by radio-loud AGN. We investigate numerically the effects that the powerful jets and continuous metal formation, of a massive galaxy in the core of a cool-core cluster, have on the hydrodynamics and chemistry of the ICM. We explore the consequences of varying the jet power, the galaxy metal distribution profile and the metal formation rates. Our implemented cluster and galaxy models are described in Section 2 along with our numerical setup. We describe and discuss our results in Section 3 and give our conclusions in Section 4. In this paper we extend the work of Heath et al. (2007). In particular, we use an improved numerical scheme (see below) which enables us to model intermittent jets as well as injection of metals from star formation.

2 THE SIMULATIONS

2.1 Numerical setup and initial conditions

We solve the equations of hydrodynamics using the Flash code (Fryxell et al. 2000) assuming axisymmetry in a 2D sphere. Given this geometry we use spherical polar coordinates (r, θ) . Flash is a well tested (Caldier et al. 2002) parallel modular hydrodynamics code with an adaptive mesh. It solves the Riemann problem using a Piecewise-Parabolic Method able to work well with contact discontinuities, making it well-suited to our current problem.

To implement the galaxy cluster we use a computational domain with ranges $r \in [0, 3000]$ kpc, without flow and hydrostatic boundary conditions at the inner and outer radii respectively, and $\theta \in [0, \pi]$ rad both with reflective boundary conditions to establish the rotational symmetry of the system. Our initial grid setup consisted of 512×16 zones which were adaptively refined by a half, attaining a maximum resolution of 2.92 kpc in the radial direction and 1.27 kpc in the angular one. Each simulation took 5 hours (on average) to run on 20 processors of the Cambridge¹ cluster of the University

of Cambridge, and the production runs were made at the Darwin² cluster of the University.

The initial conditions of our ICM gas were simulated as a monatomic hydrogen plasma with an ideal gas equation of state ($\gamma = 5/3$), an initial constant temperature of 10^7 K and a King density profile (King 1972):

$$\rho(r) = \frac{\rho_0}{(1 + (r/a_0)^2)^{3/2}}; \quad (1)$$

We set the cluster's core density, ρ_0 , and radius, a_0 , to be $10^{-23} \text{ kg m}^{-3}$ and 100 kpc respectively, and take $\gamma = 2/3$. For this initial gas distribution to be in hydrostatic equilibrium, the gravitational acceleration of the dark matter potential well must satisfy:

$$g_r = -\frac{3 k_B T}{m_H a_0^2} \frac{r}{(1 + (r/a_0)^2)^2}; \quad (2)$$

where $\gamma = 1/2$ and m_H is the proton mass. We neglect the self-gravity of the cluster gas and take this as a fixed background gravitational field.

We include an energy loss term, $dE = dt$, to account for the ICM radiative cooling due to Bremsstrahlung:

$$dE = dt = -1.722 \times 10^{-40} \frac{n^2}{\text{m}^3} \frac{r}{\text{K}} \frac{T}{\text{W m}^3}; \quad (3)$$

Our simulations consist of three phases: (1) The cooling flow phase, in which we let the initial ICM to evolve subject to Bremsstrahlung radiation and gravity only, until it reaches a quasi-steady state. The system then develops a nearly spherically symmetric inflow. (2) The radio galaxy active phase(s), when we use the $\theta \in [0.5, 0.5]$ rad region of the inner radial boundary (with $r = 10$ kpc) to inject two light jets into the cluster with a velocity of a third of the speed of light (Lorentz factor = 1.048). We set the density of the jets to be 10^{-3} times smaller than the initial central ICM density, and the pressure of the jets was adjusted to that of the cooled central ICM of $2.2 \times 10^{-17} \text{ N m}^{-2}$. This simulates a powerful FR II (Fanaro & Riley 1974) radio source with a jet power of $8.8 \times 10^{39} \text{ W}$ atts. (3) The remnant phase, during which the ICM, the metals (see the following Section) and the convective flows left by the jets evolve passively, under the influence of gravity and Bremsstrahlung radiation, for 3 Gyr. Our different simulations and parameters are summarised in Table 1.

2.2 The tracer fields, conservation and injection

We implement the distribution and evolution of metals using Flash's tracer fields (fields from now on). The metallicity, Z , is the ratio of the metal density to the ICM gas density, $Z(\mathbf{x}) = \rho_m(\mathbf{x})/\rho_g(\mathbf{x})$, and the field is defined so that:

$$f(\mathbf{x}) = N Z(\mathbf{x}); \quad (4)$$

where N is a constant factor required by Flash to keep $f \in [0, 1]$. Flash uses two fields: f , representing the metal distribution, and f , the non-metal gas fraction. Then, fields are conserved in the sense that $f + f = 1$ in every zone of the simulation grid. Thus, normalisation parameters are required to fulfil this condition.

¹ www.esience.cam.ac.uk/projects/cam-grid/

² <http://www.hpc.cam.ac.uk/darwin.html>

Table 1. Simulations and parameters. The names of the simulations contain the information about the time between the jet outburst (interludes, I), the metal injection replacement time (R) and a letter P when the central galaxy metal distribution is implemented with a Plummer profile.

Simulation name	Number of jet episodes	Duration of each outburst [Myr]	Time between outbursts [Myr]	Injection replacement time t_c [Myr]	Metal distribution profile
I0-R Inf	1	30	0	1	at
I0-R 1000	1	30	0	1000	at
I0-R 500	1	30	0	500	at
I10-R Inf	3	10	10	1	at
I100-R Inf	3	10	100	1	at
I100-R 1000	3	10	100	1000	at
I100-R 500	3	10	100	500	at
I100-R Inf-P	3	10	100	1	Plummer
I100-R 1000-P	3	10	100	1000	Plummer
I0-R 500-P	1	30	0	500	Plummer
I100-R 500-P	3	10	100	500	Plummer

We use two galaxy metal density distributions: a flat distribution:

$$\rho_g = \begin{cases} \text{for } r \leq [10; 50] \text{ kpc;} \\ 0 & \text{elsewhere;} \end{cases} \quad (5)$$

and a Plummer-like distribution (see Table 1):

$$\rho_{mP}(r) = \frac{\rho_P}{(1 + (r/r_c)^2)^{5/2}}; \quad (6)$$

where r_c in the denominator of equation (6) is the core radius of the galaxy metal distribution, which we set to 15 kpc. The metal density, ρ_P , in equation (6) was adjusted to be equal to ρ_0 (equation 1) making the metal density, $\rho_{mP}(r)$, a reasonable and arbitrary fraction of the ICM gas. On the other hand, ρ_g , in equation (5), was adjusted so that the initial metal mass in the cluster is the same for all our simulations.

Metals are injected via star formation which we consider only in the central dominant cluster galaxy. To simulate this process (from phase 2 of the simulation onwards) we add metals to the ICM gas, with a radial dependence following the initial metal distribution (either $\rho_g(r)$ or $\rho_{mP}(r)$ (equations 5 or 6 respectively)) with a metal replacement time, t_c , so that:

$$\frac{d\rho_m(r;t)}{dt} = \frac{\rho_m(r)}{t_c}; \quad \frac{d\rho_g(r;t)}{dt} = \frac{\rho_g(r)}{t_c}; \quad (7)$$

Values for t_c (see Table 1), are based on previous work which consider a constant star formation rate David et al. 2001; Gaibler, Krause & Camenzind 2005. From equations (7) the computational Euler step for these densities is given by:

$$\begin{aligned} \rho_m^{n+1}(r;t) &= \rho_m^n(r;t) + \rho_m(r) (dt=t_c); \\ \rho_g^{n+1}(r;t) &= \rho_g^n(r;t) + \rho_g(r) (dt=t_c); \end{aligned} \quad (8)$$

where $n+1$ denotes the densities at the current time step, dt , and n , the densities at the previous time step. The evolution of the metallicity is hence given by equations (4) and (8):

$$Z^{n+1}(r;t) = \frac{\rho_m^{n+1}}{\rho_g^{n+1}} = \frac{\rho_m^n + \rho_m(r) (dt=t_c)}{\rho_g^n + \rho_g(r) (dt=t_c)}; \quad (9)$$

and thus the evolution of the fields follows so that:

$$f^{n+1} = f^n - \frac{\rho_g^n}{\rho_g^n + \rho_m(r) (dt=t_c)} + \frac{N_m(r) (dt=t_c)}{\rho_g^n + \rho_m(r) (dt=t_c)}; \quad (10)$$

where f^{n+1} and f^n represent the fields for the current and the previous time steps respectively.

We tested our implementation and conservation of the fields by following the evolution of an annulus sector with a constant field distribution, during a cooling flow phase (see Section 2). We found a loss of fields due to advection of 2 parts in 10^6 over a Hubble time. The inner computational boundary has outflow boundary conditions (except for the jets' nozzles during the active phases) and thus fields (metals) can be lost only if they flow through this boundary. A similar test for our implementation of fields injection resulted in a metal loss of not more than 1%, over a Hubble time (since our simulations last for 3 Gyr, we can definitely neglect these numerical effects).

3 RESULTS AND DISCUSSION

The basic dynamical evolution observed in the simulations is as follows. During phase 1 (see Section 2) radiative cooling leads to the formation of a cooling flow. We run the simulation until the cooling flow reaches a steady state and develops a core with cooling flowing gas and a radial gradient in the velocity (this gradient is very steep near to the core and flat away from it). The initial hydrostatic equilibrium conditions prevail away from the core in agreement with canonical models (e.g., see Fabian 1994). During phase 2, the initial hydrodynamical structure of powerful jets develops. The jets drive a supersonic bow shock from the centre of the galaxy through the ICM, but at this stage the fields are not removed from the core. Behind the shock, the under-dense jets form a low density cocoon bounded by a contact surface. The jets push aside the central cool gas and metals in their way. The cocoon grows roughly self-similarly in accordance with the models of Kaiser & Alexander (1997) and Alexander (2006). The left panels in Figure 1 show the distribution of the logarithms of the density (top) and the fields (bottom), at the end of the active phase of run I0-R Inf (30 Myr). The jets, the cocoon and ambient medium are clearly visible.

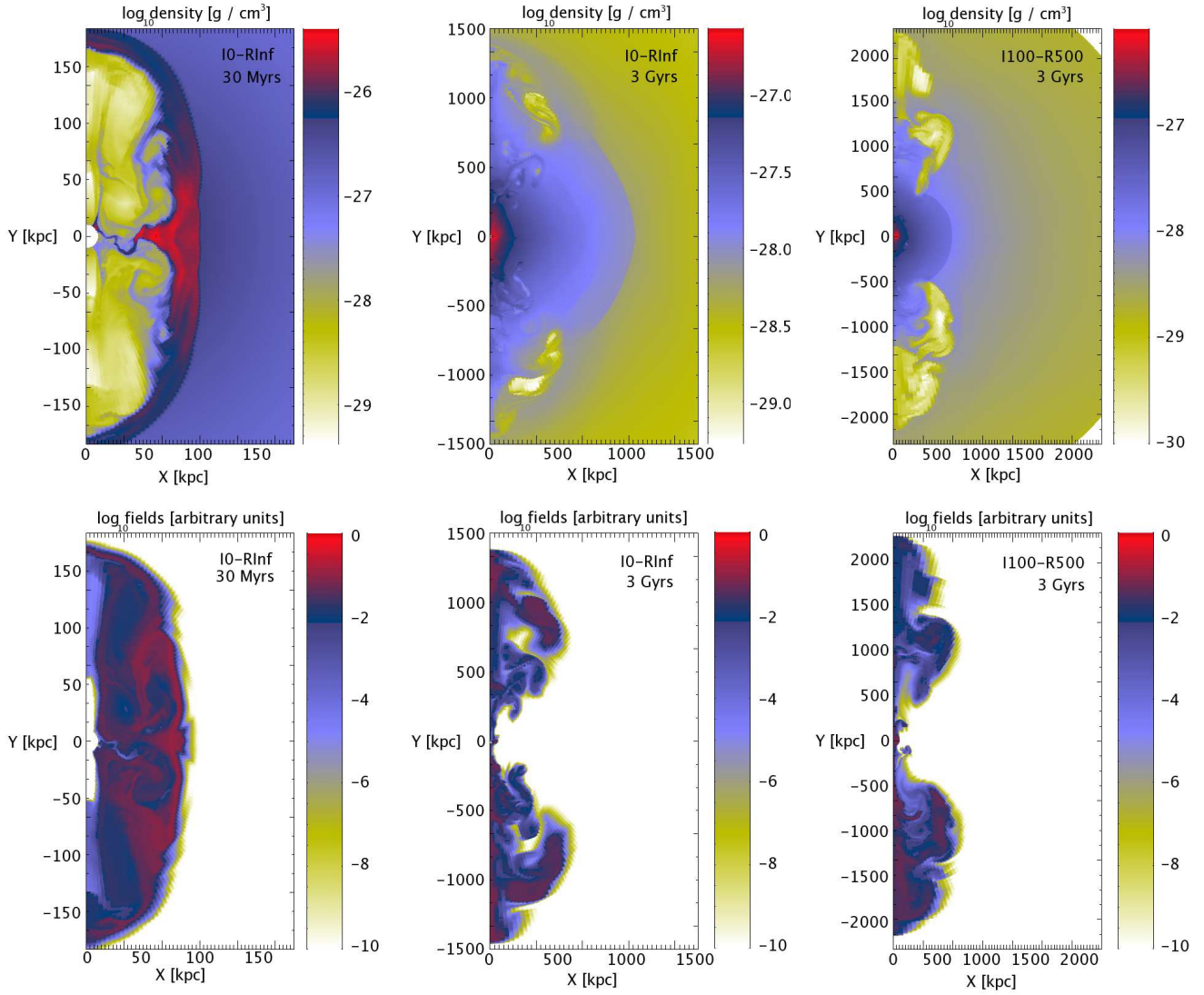


Figure 1. Plots (xy plane) of the logarithms of the ICM gas density (top) and the tracer fields (bottom). Left panel shows run I0-RInf (see Table 1) at the end of the jets' active phase. The jets and the cocoon are visible. The middle and right panels show runs I0-RInf and I100-R500 respectively, at the end of the simulation (3 Gyr).

Once the cycle of the jets is finished, the system has developed several gas layers with different densities and velocities. The expansion of the cocoon decelerates gradually. Hydrodynamic instabilities grow and disrupt the cocoon producing turbulent flows in the central ICM. The remnant cocoon forms two hot buoyant bubbles that propagate away from the core, in agreement with previous 3D hydrodynamical simulations (e.g., see Churazov et al. 2001; Basson & Alexander 2003).

The fields mimic the motion of the gas flows closely and mixing of gas with low and high metal concentrations occurs, particularly close to the most prominent turbulent vortices. The later effects are more important when intermittent jets are present (see Table 1). The convective flows drag the metals very efficiently (95% of the initial galaxy metals in general) to distances up to 2 Mpc (see Figures 1 and 2). The bow shock continues propagating, decelerates gradually and reaches the outer computational boundary

(3 Mpc) at the end of our simulations (3 Gyr). The middle and right panels in Figure 1 show the distribution of the logarithms of the density (top) and the fields (bottom), of these convective flows, at the end of the simulation for Runs I0-RInf and I100-R500.

3.1 The time evolution of the metal distribution

Figure 2 shows the (logarithm) azimuthal average of the relative metallicity of the ICM gas density, as functions of radial distance from the cluster's core at different epochs. The relative metallicity in a given shell of thickness dr is calculated as:

$$\frac{Z(r)}{Z_0} = \frac{1}{Z_0} \frac{\int_0^R \rho_m(r'; \theta) r'^2 \sin(\theta) d\theta dr'}{\int_0^R \rho_g(r'; \theta) r'^2 \sin(\theta) d\theta dr'}; \quad (11)$$

where Z_0 is an arbitrary normalisation factor which, in Section 3.2 below, we use to compare our simulated metallicity

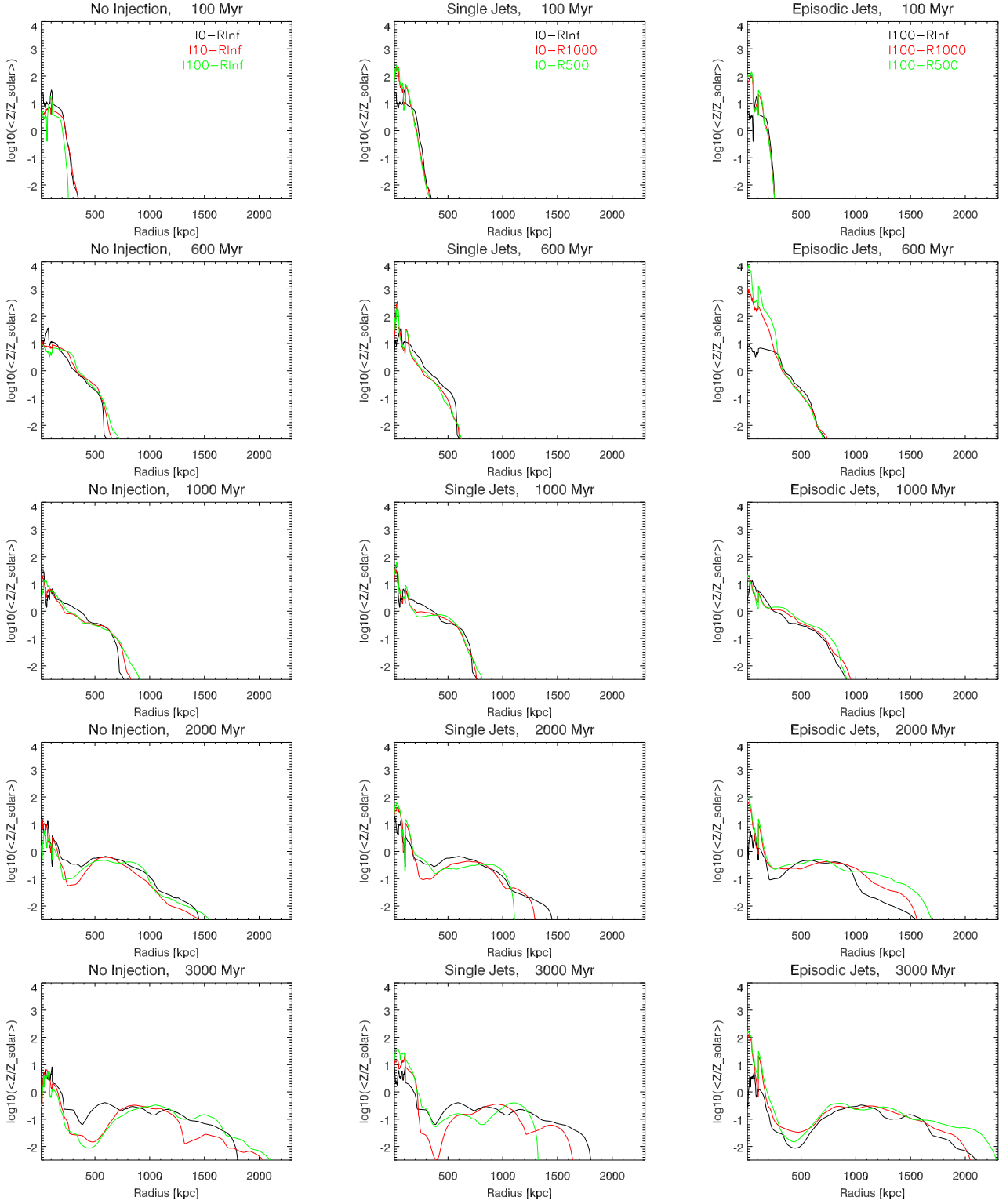


Figure 2. Time evolution of the mean relative metallicities as functions of the radius from cluster centre. Each point shows the logarithm of the azimuthal integration (spherical shells) of the ratio of the metal density over the ICM gas density (see equation 11), i.e., the mean metallicities are normalised in order to be compared with the observations (see Section 3.2). Column 1, comparison of simulations of galaxies with no metal injection and different jets' duty cycles. Column 2, comparison of Runs with a single 30 Myr outburst and different matter injection rates. Column 3, comparison of simulations with three 10 Myr outbursts (and two 100 Myr interludes) and different matter injection rates (see Table 1).

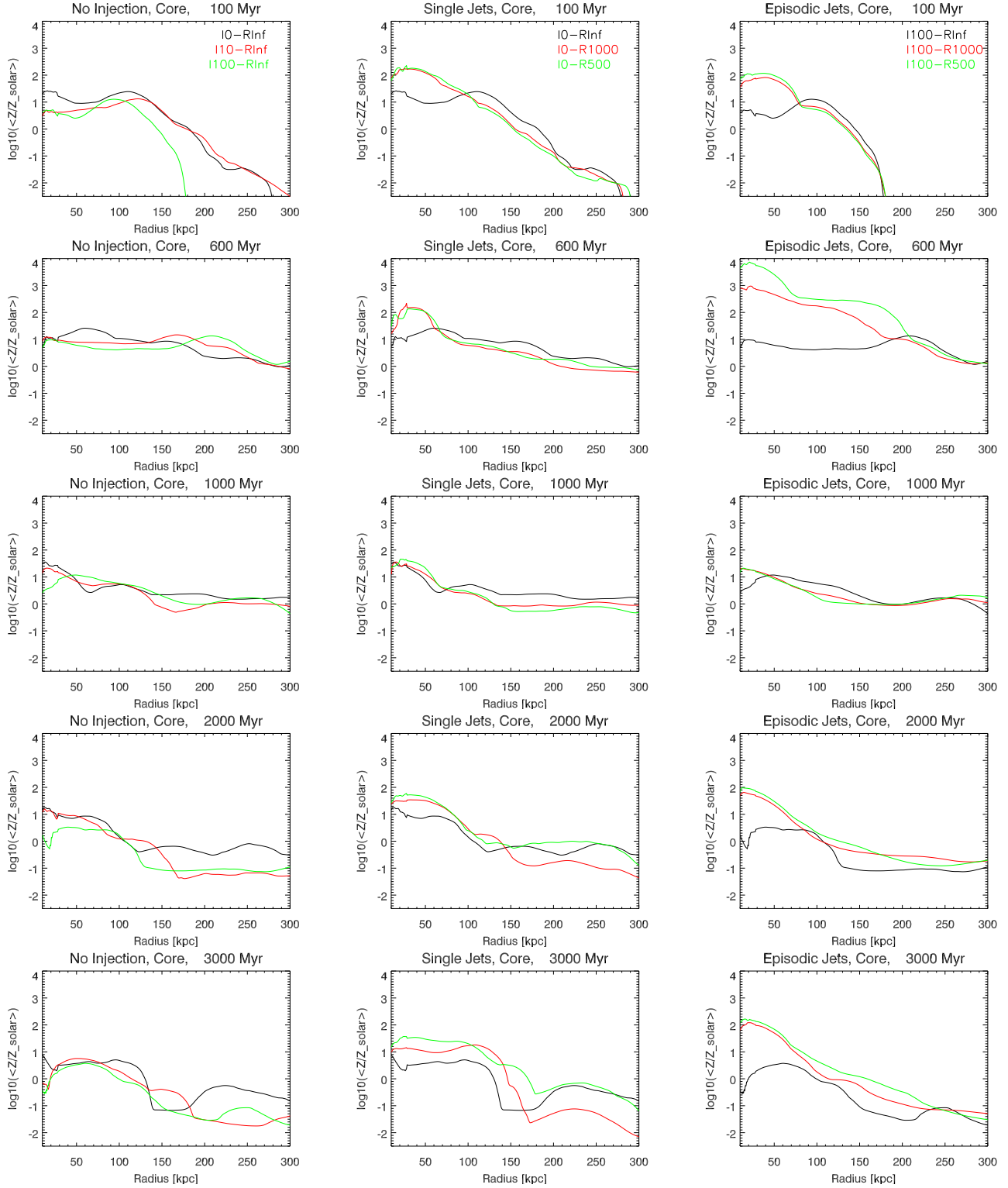


Figure 3. A zoom into the central 300 kpc of Figure 2.

gradients with the observations from *Leccardi & Molendi (2008)*. The left most column in Figure 2 (hereafter 2L) shows Runs without any metal injection and with different jet active phases. The middle column (2M) shows Runs with a single 30 Myr outburst and different metal distributions and injection rates. The right most column (2R) displays

Runs with the same episodic jets, but different injection rates (see Table 1). Furthermore, Figures 3 and 4 present plots with a similar format, arranged by columns (and we address them with the same short notation for the left middle and right columns). Figure 3 shows details of the central region of all the plots in Figure 2 while Figure 4 compares

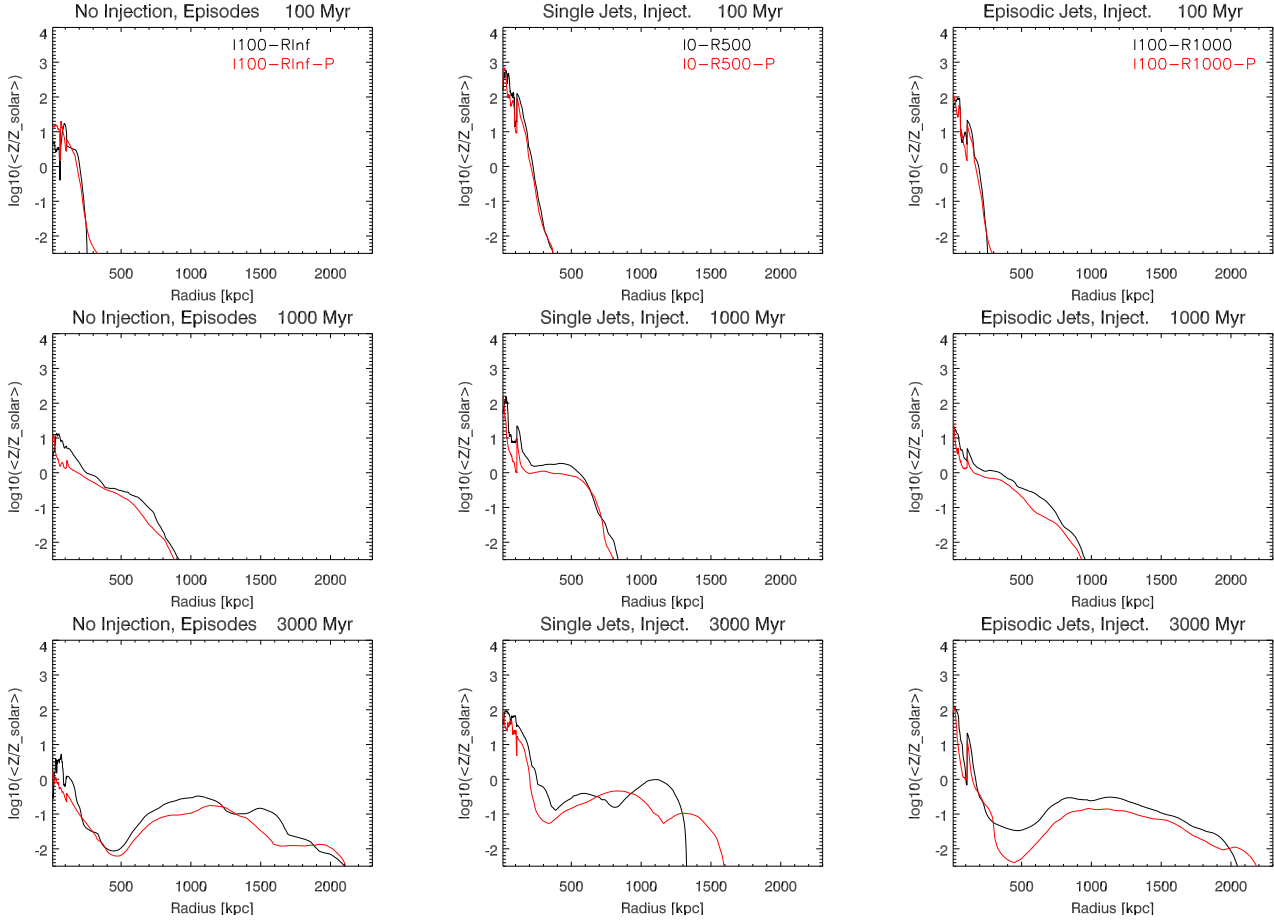


Figure 4. Time evolution of the logarithm of the mean relative metallicities showing the differences between Runs with a flat (black) and a Plummer (red) metal distributions. The dynamical evolution of the ICM metallicity is independent of the metal distribution details at the central dominant galaxy.

runs with the same parameters except for the galaxy metal distribution. It is important to note that the total AGN energy input to the ICM is the same in all cases.

Figure 2 shows that although powerful AGN jets are transitory phenomena, they produce important dynamical and chemical effects on the ICM on megaparsec scales for a few gigayears. The large-scale dynamical evolution of the ICM and its metals is similar for all our simulations (see Figures 2, 3 and 4). The initial metal distribution of the central galaxy is rapidly lost and the very steep and negative gradient of the metallicity rise slowly. The central region, $r < 250$ kpc, remains quite steep specially if metal injection is present. From 2 Gyr onwards regions with flat gradients develop for $r > 500$ kpc and for some central regions as well (see Figures 3 and 5).

The number of jet episodes has an effect from about 2 Gyr onwards, mainly within the regions $r < 200$ kpc and $r < 1500$ kpc. The metallicity profiles in Figure 2 show that after evolving for 3 Gyr, the ICM metals advected by single outburst jets (single jets) reach radii 1800 kpc from the cluster's core. However, if intermittent jets are present, metals reach 300 kpc further. On the other hand, metallicity plots, more significantly from systems with intermittent jets, show reductions in metallicity in the region $r < 200$ kpc of an order of magnitude (see Fig-

ures 2 and 5). Similar depressions were found by Heath et al. (2007) in their simulations but it is difficult to find any traces of such metal distribution gradients with current X-ray spectroscopic observations of clusters. In our simulations, gas and metals are continuously injected into the central dominant galaxy (see equation (8)) and thus the AGN relic bubbles inflated by episodic jets carry with them more metals and gas than bubbles formed by single jets do. The ICM gas in the surroundings will occupy the space left by the bubbles when they rise, producing central inflows in the cluster. These inflows are larger for episodic jets. The combined effects of these inflows (replenish central regions with metal-poor gas) and the rising bubbles (moving hot gas and metals away from the core) result in an intermediate intermediate region in the cluster, with low metallicity. Furthermore, during the intermittent jets' active phases every outburst drives an expanding shock wave leaving turbulent inflows in its wake. Shocks of secondary outbursts sweep out turbulent gas formed by previous outbursts. Thus, the hydrodynamical structures produced are more complex when intermittent jets are present, in agreement with the radio observations of intermittent jets of Brocksopp et al. (2007). These physical conditions facilitate the mixing of gases with different metal concentrations, resulting in smoother metallicity profiles as shown in the last row of Figures 2, 3 and 5.

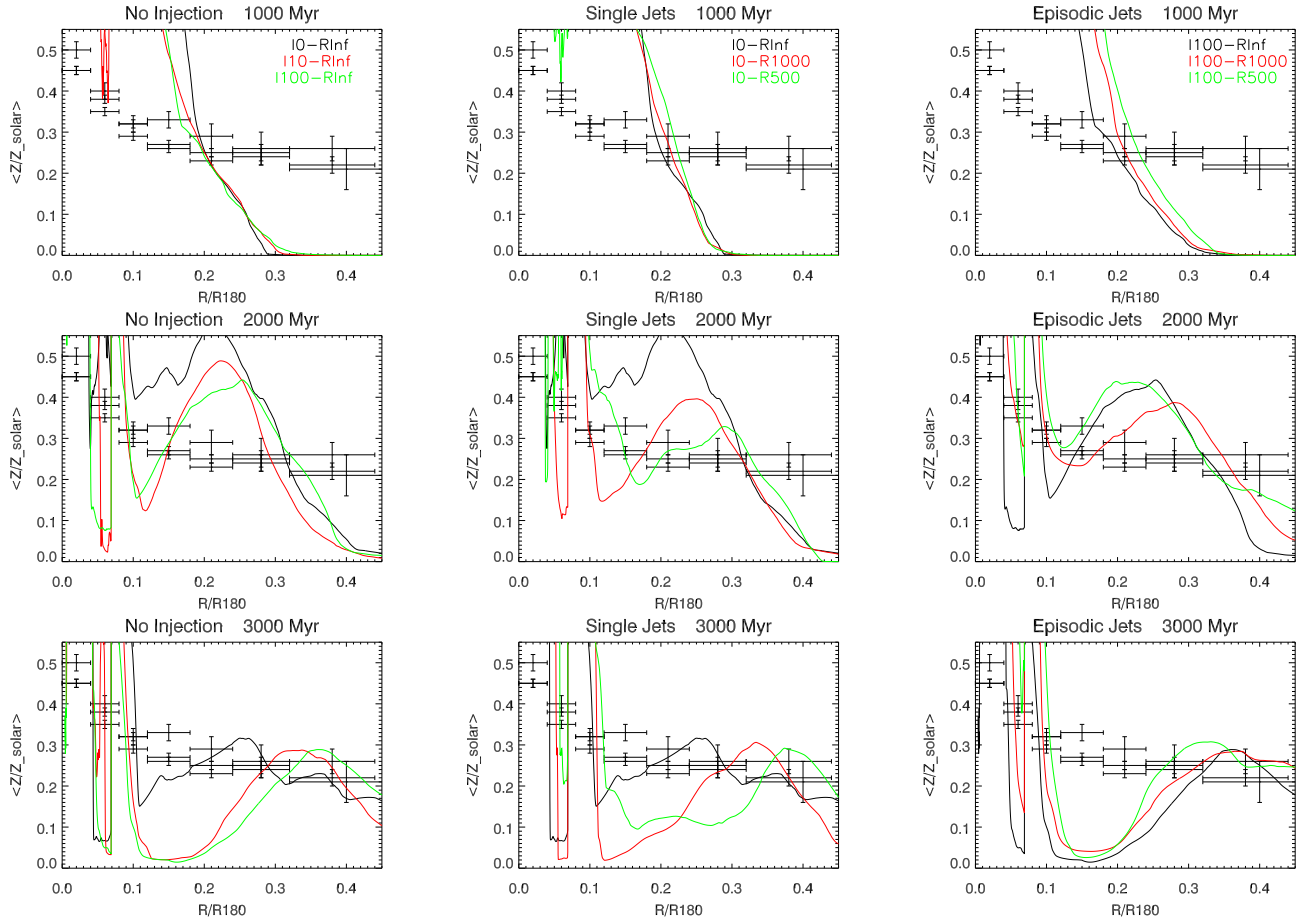


Figure 5. General evolution of the mean relative metallicities of our simulations overlaid on the ICM radial metallicity profiles from the data composition (Figure 5) by Leccardi & Molendi (2008).

The metal injection has effects on the general metal abundances present in the ICM, specially at the core (see 2M, 2R, 3M, 3R, 5M and 5R). The faster the metal replenishment time, t_c , the higher the metal abundance. Figure 3 shows that the metallicity profiles at radii ~ 75 kpc are dominated by the central galaxy. On the other hand, an important metallicity drop is evident at the core of the cluster between 600 Myr and 1 Gyr, for runs with metal injection (see 2M, 2R, 3M and 3R). This loss and redistribution of metals takes place the moment the equatorial part of the 'jets' cocoon collapses, and the formation of the buoyant bubbles of hot gas. In this process some small proportion of metals are lost in our simulations through the inner computational boundary (while others, are lifted to larger radii to form the bubbles). However, by comparing runs with and without injection in Figures 2 and 3, from 1 Gyr onwards, it seems that the rapid central metallicity changes mentioned above (between 600 Myr and 1 Gyr) have no important effects on the general metallicity evolution of the ICM.

The metal distribution details of the central galaxy (either at or Plummer, see Section 2.2) have no effect on the dynamical evolution of the ICM metallicity on large scales, as shown in Figure 4. The discrepancies in 4M at 3 Gyr (and 2M as well) are only due to numerical advection.

3.2 Comparison with Radio and X-Ray observations

As discussed above, intermittent jets drive turbulence and mixing in the ICM. Direct evidence of jets with three outburst episodes was first found in the FR II radio galaxy B0925+420 by Brocksopp et al. (2007). The ages of the lobes of this radio source (a few Myr) are comparable to the intermittency timescales we use in our simulations. Furthermore, there is observational evidence of turbulence and diffusion in the ICM, e.g., see Rebusco et al. 2006 and references therein. However, a quantitative study of the 'nested cocoons' and the ICM turbulence and diffusion is beyond the scope of this letter.

In Figure 5 we compare the mean metallicity profiles from the X-Ray data presented in Leccardi & Molendi (2008) and references therein, to our simulations at different epochs. It is evident that for radii $> 0.12 R_{180}$ our simulations present pronounced metallicity gradients that do not follow the general trends present at larger radii. In our simulations this inner region is dominated by the metals of the central galaxy (see Figures 2 and 3). We do not expect our simulations to reproduce the metallicity gradients on small scales, where the profiles are likely to be shaped by less-energetic phenomena than AGN activity such as galactic winds. Away from the core however some of our simu-

Table 2. Ranges of agreement between our simulations and the observations from Leccardi & Molendi (2008), at 3 Gyr.

Simulation name	Approximate radial range [R_{180}]
I0-R Inf	(0.18, 0.45)
I0-R 1000	(0.26, 0.40)
I0-R 500	(0.32, 0.45)
I10-R Inf	(0.27, 0.42)
I100-R Inf	(0.31, 0.45)
I100-R 1000	(0.29, 0.45)
I100-R 500	(0.25, 0.45)

simulations develop metallicity gradients comparable, over radii from 0.1 to $0.4 R_{180}$, to those in the data (see Figure 5). Table 2 summarises the radial ranges over which the mean metallicity of our simulations is in agreement with experimental data. The best fit is obtained with Run I0-R Inf, with a single jet outburst and no metal injection.

4 CONCLUSIONS

We present 2D axisymmetric hydrodynamical simulations of thermal advection in the ICM, driven by the jets of a radio-loud AGN. We implement the ICM with a cooling flow, and the central CD galaxy with a metal distribution and continuous metal formation, and powerful intermittent jets. The jets produce the early and late features typical of canonical models, simulations and observations of FR II objects (e.g., see Churazov et al. 2001; Alexander 2006; Heath et al. 2007; Brocksopp et al. 2007). We model the metals using tracer cells and explore the consequences of varying the jet intermittency, the galaxy metal distribution profile and thermal formation rates. We have found the following.

Although powerful AGN jets are transitory phenomena they produce important dynamical and chemical effects on the ICM on megaparsec scales for a few gigayears.

The convective flows formed long after the AGN active phases drag 95% of the initial metals in the central galaxy to distances $> 1.5 Mpc$.

We implement intermittent jets with the same total energy input to the ICM. The general metallicity evolution for all our simulations is very similar on large-scales: after 2 Gyr, approximately flat metallicity gradients are formed from radii 700 to 1300 kpc. Metallicity drops are formed (found by Heath et al. (2007) as well) of factors of 15 at $r2(200, 750)$ kpc. These features might be correlated to the mass of the gas and metal advected by the relic bubbles, but high resolution X-ray observations are needed to see traces of such metallicity gradients. Furthermore, intermittent jets distribute metals 300 kpc further than single outburst jets do, and also facilitate the mixing of gases with different metal concentrations and induce turbulence in the ICM.

The metal injection has effects on the general metal abundances present in the ICM: the faster the metal replenishment time the higher the metal abundance. For radii $< 0.12 R_{180}$ our simulations are dominated by the metals of the central galaxy and do not follow the general trends present at larger radii on either our simulations or the X-

ray observations. Since metal production and jets are realistic in active galaxies, metallicity gradients in the very central regions of cool core clusters are likely to be shaped by less-energetic phenomena. On the other hand, away from the core, some of our simulations (specially the one with a single jet outburst and no metal injection) develop metallicity gradients in agreement with, over particular radial ranges, the observations of Leccardi & Molendi (2008) and references therein.

We model massive central galaxies with the same total metal mass in all cases. The metal distribution details of the central galaxy have no effect on the dynamical evolution of the ICM metals.

ACKNOWLEDGEMENTS

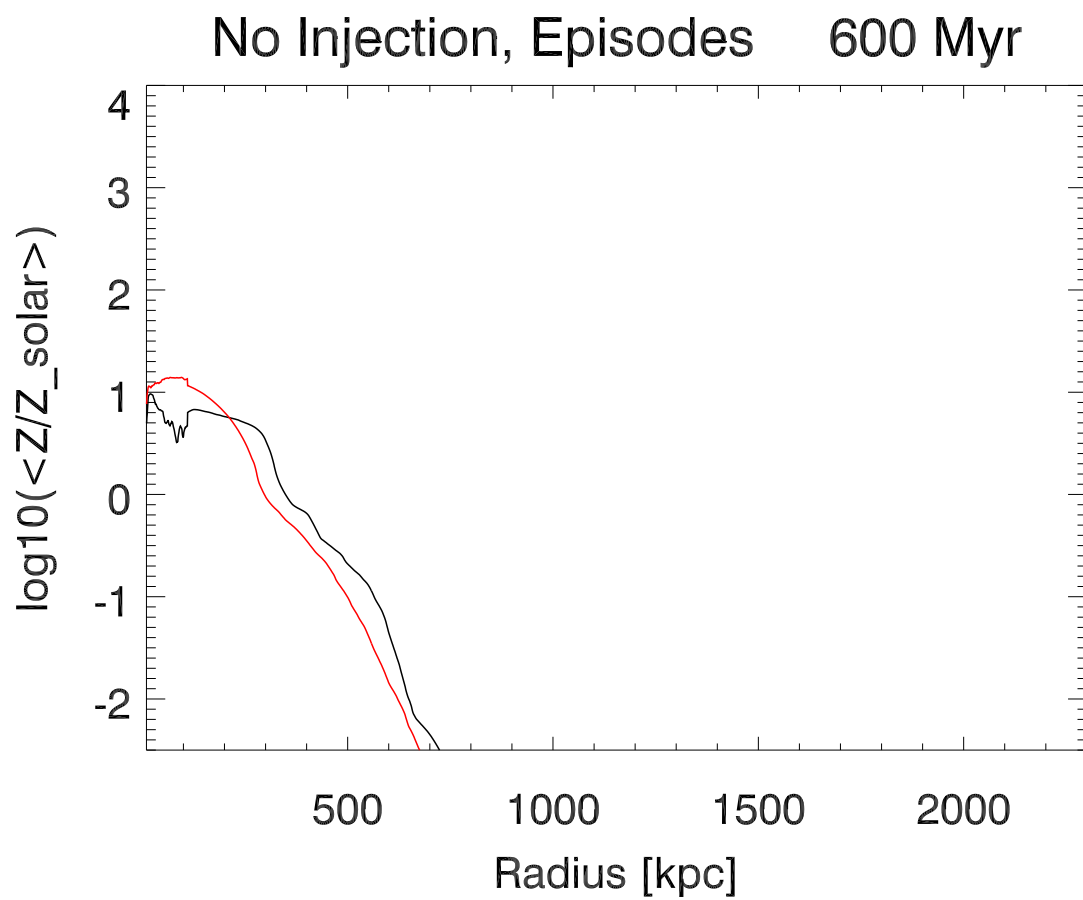
The software used in these investigations was in part developed by the DOE-supported ASC / Alliance Center for Astrophysical Thermonuclear Flashes at the University of Chicago. MHE acknowledges support from CONACyT (196898/217314).

REFERENCES

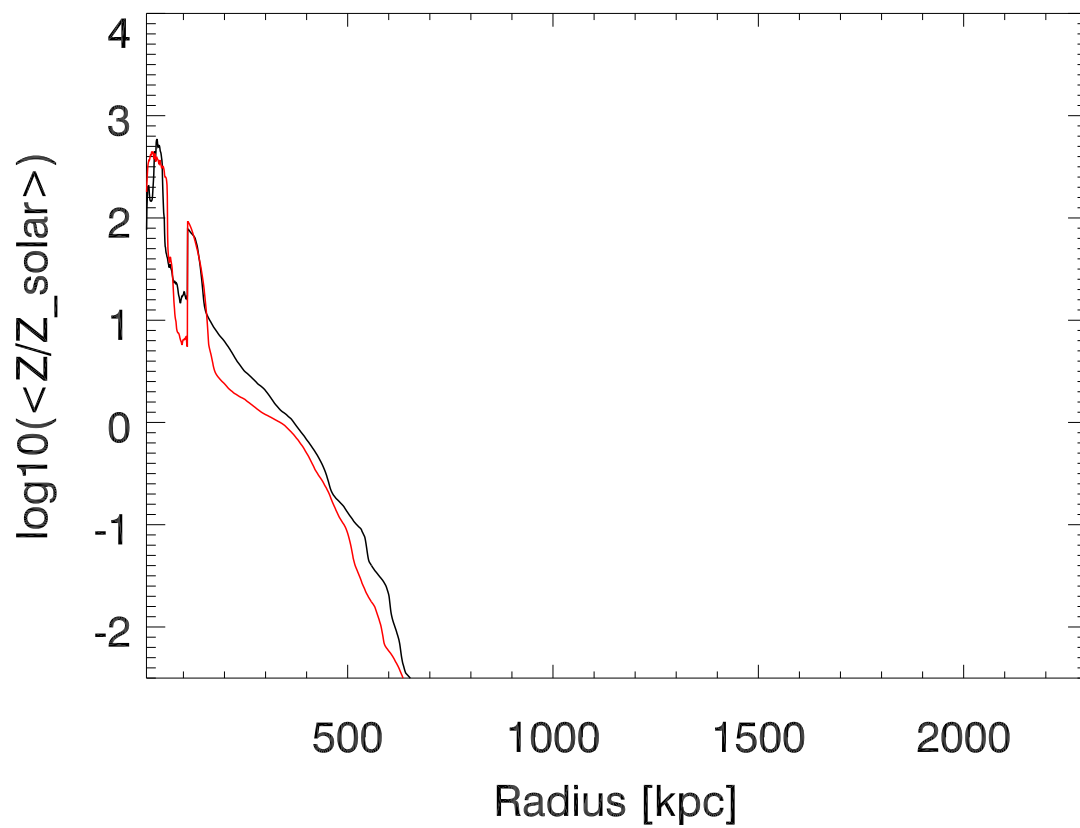
- Alexander P., 2002, *MNRAS*, 335, 610
- Alexander P., 2006, *MNRAS*, 368, 1404
- Baldi A., Ettori S., Mazzotta P., Tozzi P., Borgani S., 2007, *ApJ*, 666, 835
- Basson J. F., Alexander P., 2003, *MNRAS*, 339, 353
- Binney J., Tabor G., 1995, *MNRAS*, 276, 663
- Blanton E. L., Sarazin C. L., McNamara B. R., Wise M. W., 2001, *ApJ*, 558, L15
- Brocksopp C., Kaiser C. R., Shoenmakers A. P., de Bruyn A. G., *astroph.0709.4548v1*
- Calder A. C. et al, 2002, *ApJS*, 143, 201
- Carilli C. L. et al, 2001, eds, in *Gas and Galaxy Evolution*, Astronomical Society of the Pacific Conference Series, 240, 101
- Churazov E., Brüggen M., Kaiser C. R., Böhringer H., Forman W., 2001, *ApJ*, 554, 261
- David L. P., Nulsen P. E. J., McNamara B. R., Forman W., Jones C., Ponman T., Robertson B., Wise M., 2001, *ApJ*, 557, 546
- De Grandis S., Molendi S., 2001, *ApJ*, 551, 153
- Fabian A. C., 1994, *ARA & A*, 32, 277
- Fanaro B. L., Riley J. M., 1974, *MNRAS*, 167, 31
- Fryxell B. et al., 2000, *ApJS*, 131, 273
- Krause M., 2003, *AAP*, 398, 113
- Gabler V., Krause M., Camenzind M., 2005, preprint (*astro-ph/0502403*)
- Heath D., Krause M., Alexander P., 2007, *MNRAS*, 374, 787
- Kaiser C. R., Alexander P., 1997, *MNRAS*, 286, 215
- Kaiser C. R., Alexander P., 1999, *MNRAS*, 305, 707
- Kaiser C. R., Binney J., 2003, *MNRAS*, 338, 837
- Kaiser C. R., Pavlovski G., Pope E. C. D., Fangohr H., 2005, *MNRAS*, 359, 493
- King I. R., 1972, *ApJL*, 174, L123+
- Leccardi A., Molendi S., 2008, *AAP*, 487, 461
- McNamara B. R., Nulsen P. E. J., 2007, *ARA & A*, 45, 117

- Molendi S., 2004, eds, APIC onf. Proc. 703, Plasmas in the Laboratory and in the Universe: New Insights and New Challenges, 345 American Institute of Physics, Melville, USA
- Mushotzky R. F., Loewenstein M., 1997, ApJ, 481, L63
- Renzini A., 2004, in Mulchaey J. S., Dressler A., Oemler A., eds, in Clusters of Galaxies: Probes of Cosmological Structure and Galaxy Evolution, 261, Cambridge University Press, Cambridge, UK
- Rebusco P., Churazov E., Bohringer H., Forman W., 2006, MNRAS, 372, 1840
- Reynolds C. S., Heinz S., Begelman M. C., 2001, ApJ, 549, L179
- Shabala S. S., Ash S., Alexander P., Riley J. M., 2008, MNRAS, 739

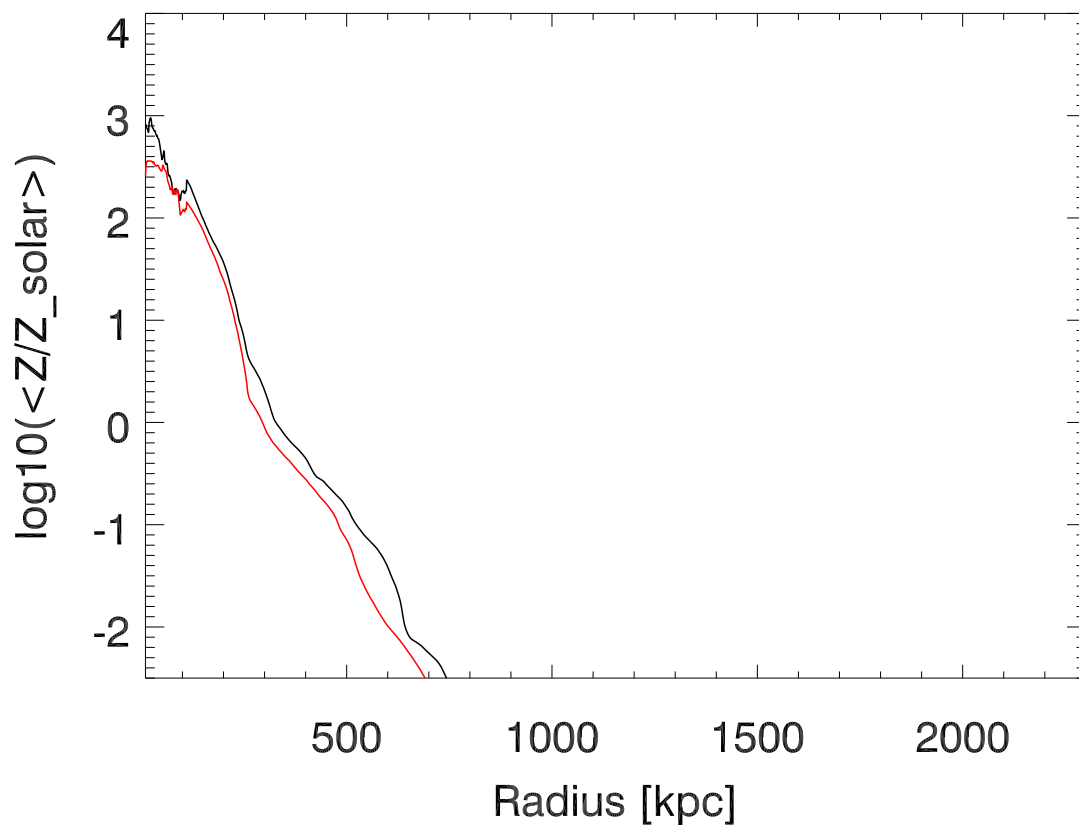
This paper has been typeset from a \LaTeX / \LaTeX file prepared by the author.

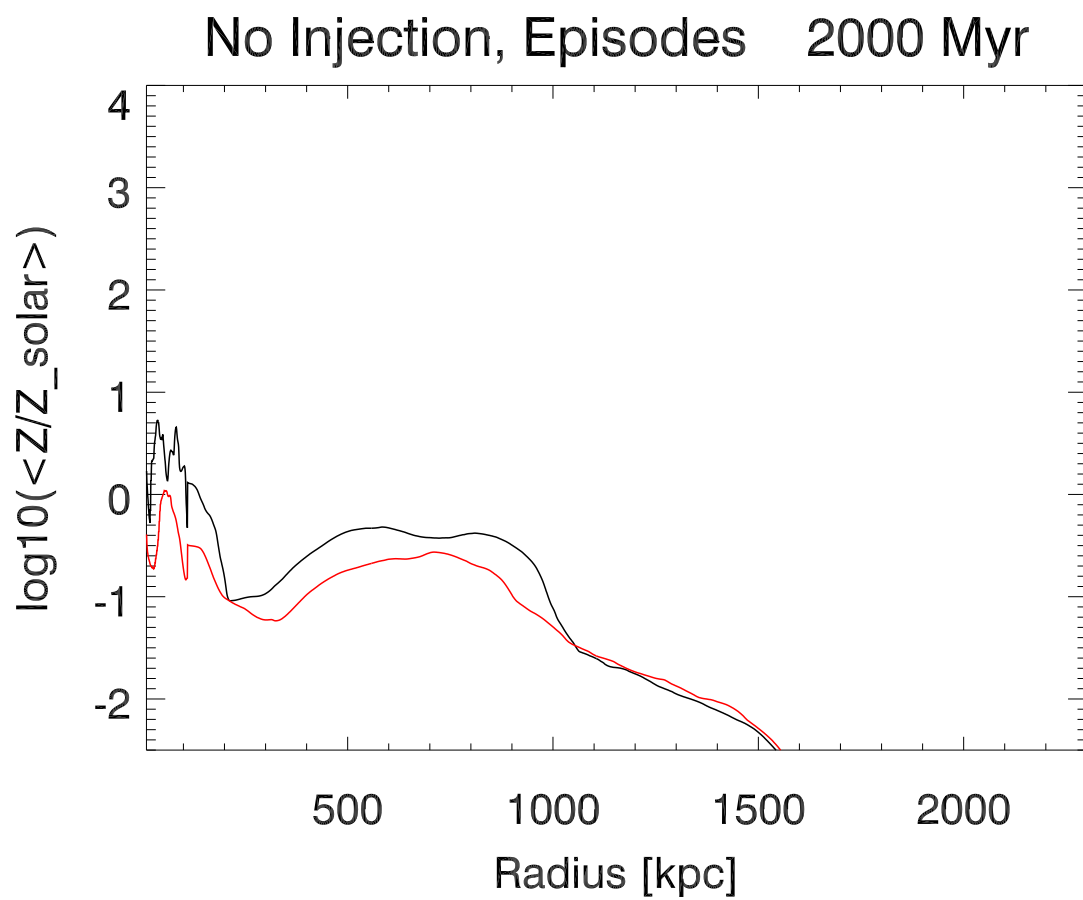


Single Jets, Inject. 600 Myr

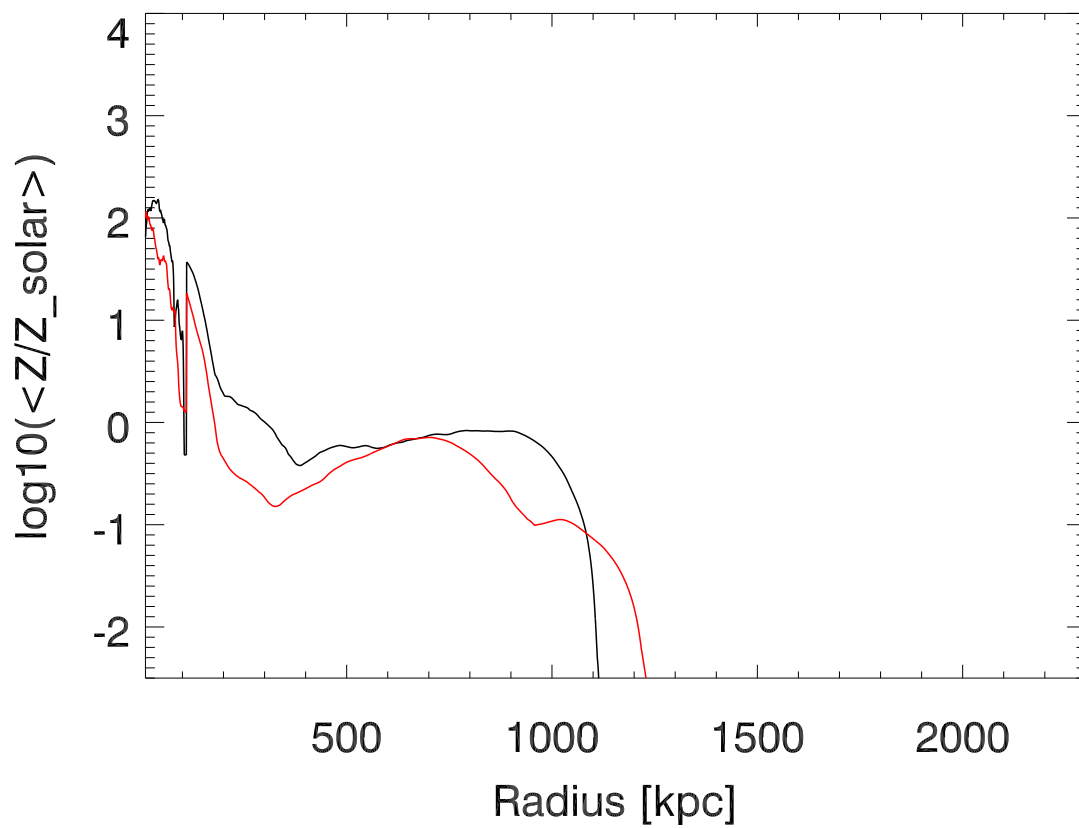


Episodic Jets, Inject. 600 Myr

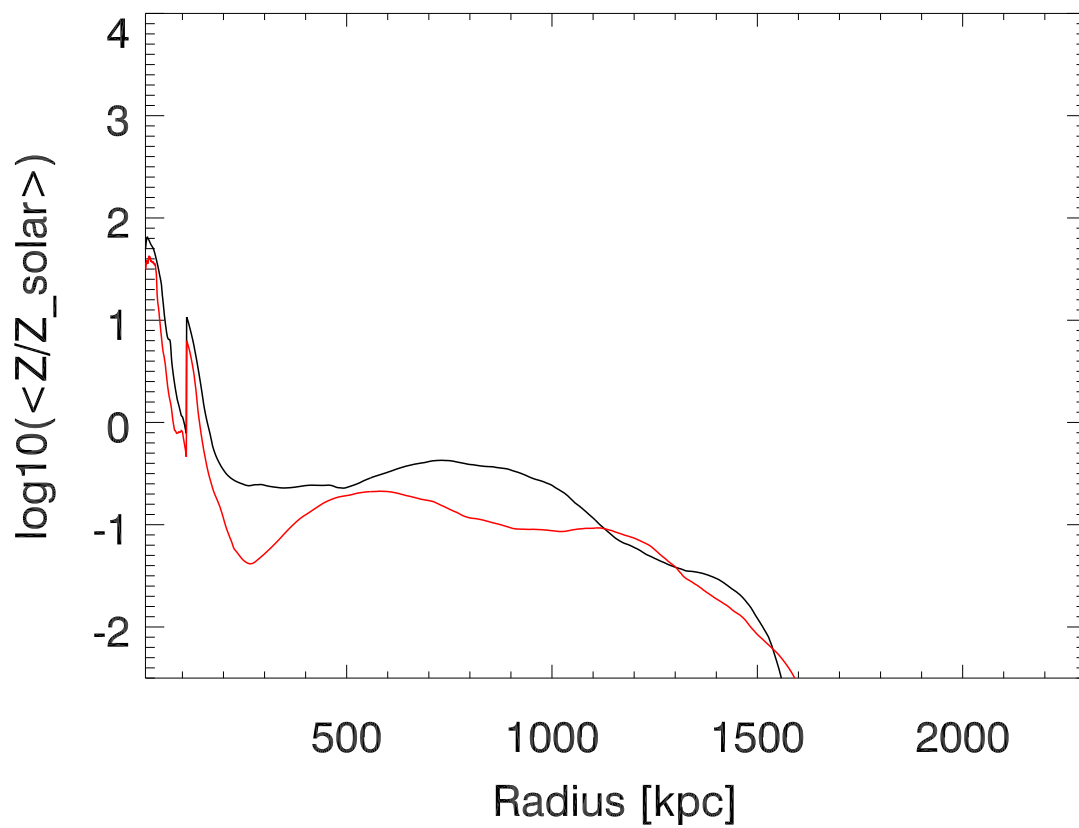




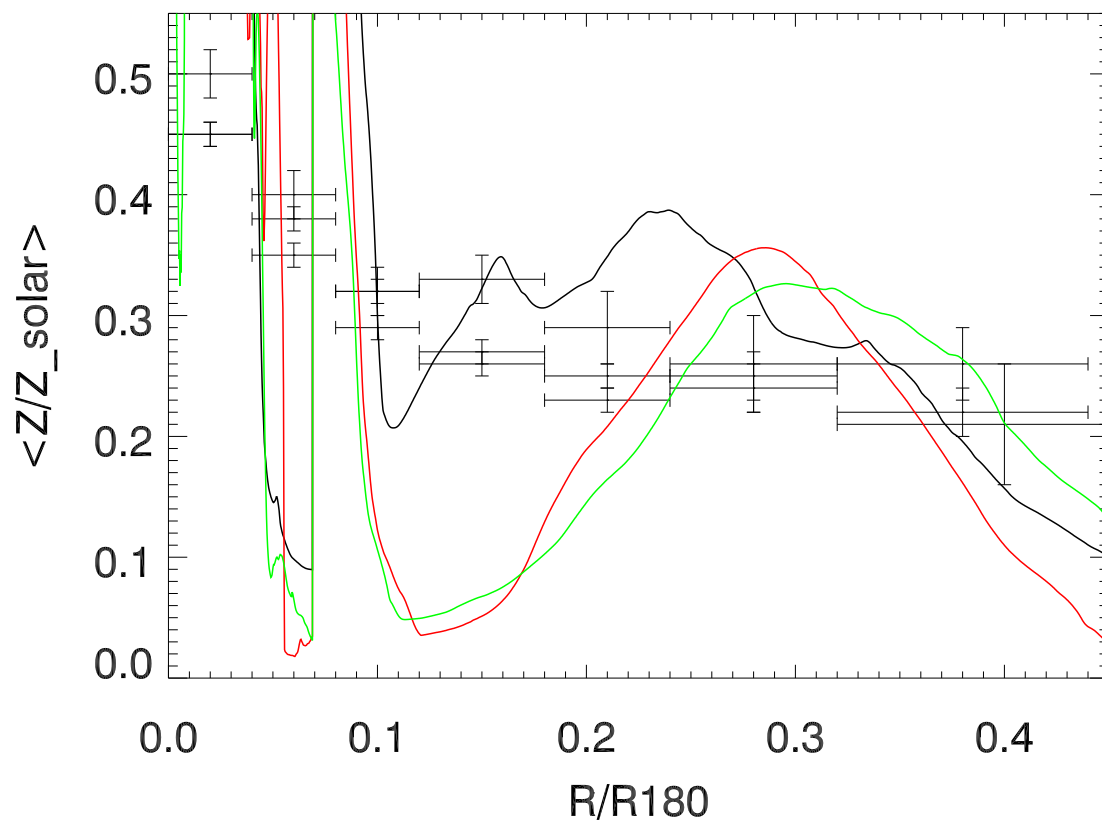
Single Jets, Inject. 2000 Myr



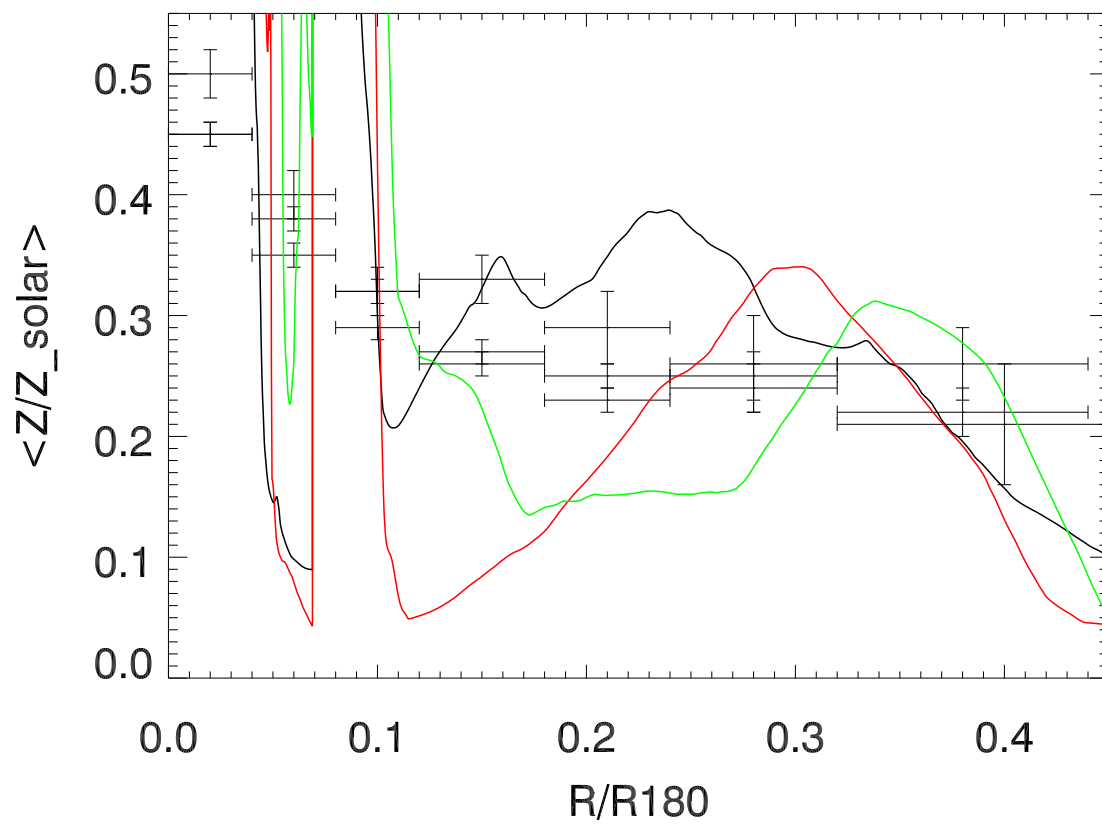
Episodic Jets, Inject. 2000 Myr



No Injection 2500 Myr



Single Jets 2500 Myr



Episodic Jets 2500 Myr

